Springer

KSME

Journal of Mechanical Science and Technology 32 (7) (2018) 3065~3072
www.springerlink.com/content/1738-494x(Print)/1976-3824(Online)
DOI 10.1007/s12206-018-0609-7

Dynamic analysis of the wind turbine drivetrain considering shaft bending effect †

Wei Shi[1,2,3,#,*], Yonghui Park[4,#], Hyunchul Park[5] and Dezhi Ning[2,3]

[1]*State Key Laboratory of Coastal and Offshore Engineering, Dalian University of Technology, No.2 Linggong Road, Ganjingzi District, Dalian, 116024, China*
[2]*Deepwater Engineering Research Center, Dalian University of Technology, No. 2 Linggong Road, Ganjingzi District, Dalian, 116024, China*
[3]*Ocean Engineering Joint Research Center of DUT-UWA, DUT, No. 2 Linggong Road, Ganjingzi District, Dalian, 116024, China*
[4]*Pohang Institute of Metal Industry Advancement, 56, Jigok-ro, Namgu, Pohang 37666, Korea*
[5]*Graduate School of Engineering Mastership, POSTECH, San 31, Hyoja-dong, Nam-gu, Pohang 790784, Korea*

(Manuscript Received August 10, 2017; Revised January 23, 2018; Accepted March 20, 2018)

Abstract

In the previous research, shaft torsional flexibility was only considered in the wind turbine drivetrain. However, if shaft is longer and thinner than other parts, two components which are connected by shaft affect each other by rotation about bending axis. It means that there are deflections of shaft about not only torsional direction but also bending direction. In this research, we introduced spherical joint which have 3 spring stiffness about all rotational axis to define shaft. And we analyzed that how shaft bending affect drivetrain rotation, translation motion and gear mesh contact force. To do these processes, we simulated the 3-dimensional wind turbine drive train model which has bearing stiffness, gear mesh stiffness, and shaft flexibility. The gear mesh stiffness was defined by Fourier series. And the equation of motion was acquired by Lagrange equation and kinematical constraints to represent shaft flexibility. About numerical analysis, the Newmark method was used to get results. Lastly, fast Fourier transform which converts results from time domain to frequency was used.

Keywords: Structural analysis; Drive-train; Dynamics; Fourier transform; Shaft flexibility

1. Introduction

In the energy crisis, many countries have been researched alternative energy. The republic of Korea is investigating offshore wind turbine installation and developing lots of efficient ways. The wind turbine is composed of blades, nacelle, hub, and tower. In the wind industry, developing more light and stable structure have considered significantly, especially blades. However, the most important characteristic is rotation. From rotation of rotor, the drive train delivers torque to produce electricity. From this fact, we can guess that the power production is directly connected to the characteristic of drive train. Lots of effect have been devoted to study the vibration mechanisms of the pitch, yaw and drivetrain systems [1-3].

In this research, we considered the 3-dimensional drive train which has gear mesh, bearing and shaft bending effect to see influences. In the previous research, the torsional model which has gear mesh [4] and more detailed 3-dimensional model which considered location and stiffness of bearing [5] were modeled. The common concept of two researches is analyzing the vibrational results from gear mesh. If there is external torque, gear contact will take place repeatedly. So, the main characteristic of rotation can be determined by contact force. The two researches showed contact force in time and frequency domain. However, these just defined shaft as rigid component except rotational direction. It means that there is no coupled motion between two components which are connected by shaft.

Actually, the rotation can affect not only itself but also relative component because of the bearing. This phenomenon will be frequently happen if defects of gear teeth, eccentricities exist. As a result, degree of freedom about bending direction should be defined to express precious mathematical model [6].

To represent detailed shaft, we used the Timoshenko beam theory which can define torsional, translational, and bending deflection by stiffness in the beam including the tower, blade, and shaft. From this stiffness, we established the mathematical wind turbine model and compared the results to torsional drive train model to see how gear mesh, bearing, and shaft bending affect the whole system.

*Corresponding author. Tel.: +86 411 8470 6652
E-mail address: weishi@dlut.edu.cn
#These authors equally contributed to this work as first author.
† Recommended by Associate Editor Junhong Park

2. Mathematical model

2.1 Gear mesh

In the drivetrain, each component rotates according relative angular velocity. This phenomenon is determined by the gear mesh. The gear mesh was modeled by spring stiffness. Generally, the spring has constant stiffness and offer reaction force by relative displacement of two contact point. However, it can be represented as periodic change in the gear. According machine components design, the gear mesh stiffness is determined by angle of attack and contact ratios. Through this fact, we defined the gear mesh stiffness using gear angular velocity and contact ratio [4, 7]. In this research, we used rotor's angular velocity, 6 rpm, as reference. And we didn't consider damping and clearance nonlinearity. According reference, velocities of other components are determined automatically. So, the average angular velocity in the planetary stage and parallel stages were defined by Eqs. (1)-(3). We defined these angular velocities as the gear mesh frequencies. The gear mesh frequency is represented in the frequency domain. It can give the evidence of gear failures, eccentric gears, gear-mesh wear, and improper backlash.

$$\omega_M^{(P)} = \omega_C N_r \tag{1}$$

$$\omega_M^{(g12)} = \omega_{g1} N_{g1} \tag{2}$$

$$\omega_M^{(g34)} = \omega_{g3} N_{g3} . \tag{3}$$

And using the Fourier series, we established the gear mesh stiffness. Eqs. (4) and (5) are gear mesh stiffness of planetary gear stage and Fig. 1 is plot of equations.

$$k_{sp}(t) = k_{sp} + \frac{k_{sp}}{C_{sp}} \sum_{l=0}^{\infty} (a_{sp}^{(l)} \sin(\omega_M^{(p)} t) + b_{sp}^{(l)} \cos(\omega_M^{(p)} t)) \tag{4}$$

$$k_{rp}(t) = k_{rp} + \frac{k_{rp}}{C_{rp}} \sum_{l=0}^{\infty} (a_{rp}^{(l)} \sin(\omega_M^{(p)} t) + b_{rp}^{(l)} \cos(\omega_M^{(p)} t)) . \tag{5}$$

k_{sp} and k_{rp} are reference values [5].
The coefficients in Eqs. (4) and (5) are:

$$a_{sp}^{(l)} = -\frac{2}{l\pi} \sin[l\pi(C_{sp} - 2\gamma_{sp})] \sin(l\pi C_{sp}) \tag{6}$$

$$b_{sp}^{(l)} = -\frac{2}{l\pi} \cos[l\pi(C_{sp} - 2\gamma_{sp})] \sin(l\pi C_{sp}) \tag{7}$$

$$a_{rp}^{(l)} = -\frac{2}{l\pi} \sin[l\pi(C_{sp} - 2\gamma_{sp} - 2\gamma_{rs})] \sin(l\pi C_{rp}) \tag{8}$$

$$b_{rp}^{(l)} = -\frac{2}{l\pi} \cos[l\pi(C_{rp} - 2\gamma_{rp} - 2\gamma_{rs})] \sin(l\pi C_{rp}) . \tag{9}$$

Without loss of generality, it can be accepted that mesh phasing γ_i is 0. We defined 4 gear mesh model which are fifteenth order Fourier series. The general processes of establishing gear mesh are same in the planetary gear stage and parallel gear stage. But, different gear mesh frequencies and contact ratios values should be considered.

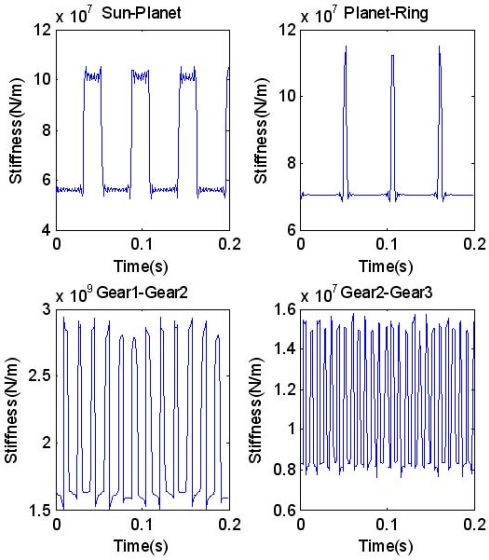

Fig. 1. Gear mesh stiffness.

2.2 Equation of motion using multi-body dynamics

As shown in Fig. 2, the wind turbine drivetrain was defined into rotor, carrier, planetary stage, parallel stages, and generator [8-15]. Each component was considered as rigid body.

There are three main shafts which exist between rotor and carrier, sun gear and gear 1, gear 3 and generator. The system properties including moment of inertia, mass and stiffness were used from previous research [4]. The equation of motion was represented by mass, stiffness, and damping matrix. Especially, mass, stiffness matrix is related to each moment of inertia, mass and relative displacement of two points which are connected by spring stiffness.

In case of shaft, it was modeled as connection of two rigid bodies which have 5 degree freedom including bending, torsional displacement. In other words, the spherical joint concept was used to define shaft deflection including torsion, bend. The spherical joint permit 3 generalized coordinates including rotation about x, y, z axis. For example, the manipulators, which are connected by links and spherical joints, consequently deflect same motion as beam without extension in the robotics. In the drive train system, the extension about z-axis of shaft can be negligible compared to rotational deflection. Using this concept, we defined shaft as 2 links which are connected by spherical joints in the center of links. Also we designated 3 springs about spherical generalized coordinates to express shaft torsional, bending deflection using the Timoshenko beam theory [16, 17].

Eqs. (10) and (11) show the Timoshenko beam's potential energy using elastic continuum and spring potential energy defined as beam model. In Eq. (11), δ is number of beam division, and k_y is spring stiffness. If we assumed that these potential energies are same, we can get the spring-beam model.

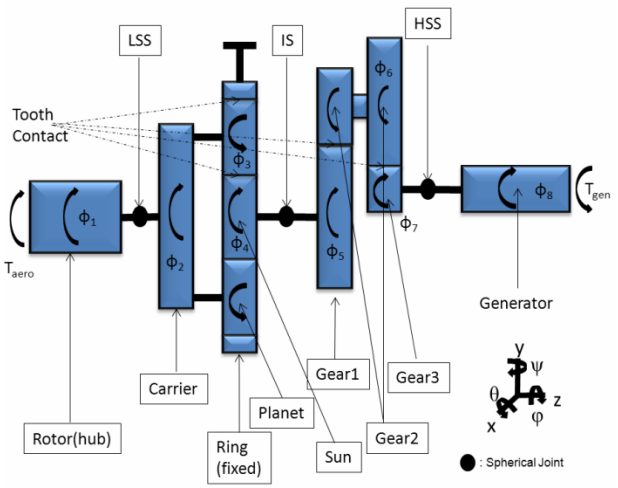

Fig. 2. Mathematical model of wind turbine drive-train.

Using this theory and reference properties including torsional stiffness, we defined the bending stiffness of shafts.

$$W_T = \frac{1}{2EI_y}\int_0^L M^2(z)dz + \frac{1}{2GA_s}\int_0^L F_s^2(z)dz = \frac{F^2L^3}{6EI_y} + \frac{F^2L}{2GA_s} \tag{10}$$

$$W_k = \frac{1}{2}k_y(((1-\delta)\frac{FL}{k_y})^2 + (\delta\frac{FL}{k_y})^2) = \frac{F^2L^2}{2k_y}[(1-\delta)^2 + (\delta)^2]. \tag{11}$$

In gear part, the gear mesh stiffness was established and composed in stiffness matrix. Not like shaft stiffness, the gear mesh stiffness is always changing according time. About gear force relations, two contact points meet and fall away by giving contact force. Through this contact force, gear will rotate. In dynamics, the potential energy of spring is expressed by relative displacement of two points and stiffness.

To derive the equation of motion, Lagrange's equation method was used [18, 19]. It is more efficient using Lagrange's equation in the constrained system. In defining system properties, gear mesh stiffness changes in every time. So we reflected these changes in stiffness matrix. About relative displacement, we showed examples of displacements related to rotation about z-axis in Eqs. (12)-(18).

$$\phi_{LSS} = \phi_{rotor} - \phi_{carrier} \tag{12}$$

$$\delta_{planet-sun} = -r_{carrier}\phi_{carrier} + r_{planet}\phi_{planet} + r_{sun}\phi_{sun} \tag{13}$$

$$\delta_{planet-ring} = r_{carrier}\phi_{carrier} + r_{planet}\phi_{planet} \tag{14}$$

$$\phi_{IS} = \phi_{sun} - \phi_{G1} \tag{15}$$

$$\delta_{G1-G2} = r_{G1}\phi_{G1} + r_{G2}\phi_{G2} \tag{16}$$

$$\delta_{G2-G3} = r_{G2}\phi_{G2} + r_{G3}\phi_{G3} \tag{17}$$

$$\phi_{HSS} = \phi_{G3} - \phi_{GN}. \tag{18}$$

Eqs. (13) and (14) are total kinetic, potential energy in the system. In Eq. (13), eccentricities in kinetic energy term was included by using radius, a_1, b_1, c_1, d_1, e_1, f_1, g_1, h_1. These eccentricities terms were from theory that center of mass can be expressed by distance from rotation axis, and cosine, sine according rotational displacement, if there is mismatch of center of mass and rotation axis.

If center of mass is not equal body fixed frame, there is distance and can be handled as radius. But, in this research, all radius terms are zero to see effects of shaft bending clearly.

In Eq. (20), all terms were multiplied by stiffness and relative displacements. As you can see, k_{LSSx}, k_{LSSy}, k_{LSSz} are LSS bending, torsional stiffness. These variable expressions are same in IS, HSS. k_{rp}, k_{sp}, k_{g12}, k_{g34} are gear mesh stiffness. And k_b is bearing stiffness. These variables are defined, expressed in Table 1.

$$\begin{aligned}
T = {} & \frac{1}{2}m_r\left[\left(\dot{x}_r - a_1\omega_r\sin(\omega_r t)\right)^2 + \left(\dot{y}_r + a_1\omega_r\cos(\omega_r t)\right)^2\right] \\
& + \frac{1}{2}J_{r_x}\left(\dot{\theta}_r\right)^2 + \frac{1}{2}J_{r_y}\left(\dot{\psi}_r\right)^2 + \frac{1}{2}J_{r_z}\left(\dot{\phi}_r\right)^2 \\
& + \frac{1}{2}m_c\left[\left(\dot{x}_c - b_1\omega_c\sin(\omega_c t)\right)^2 + \left(\dot{y}_c + b_1\omega_c\cos(\omega_c t)\right)^2\right] \\
& + \frac{1}{2}J_{c_x}\left(\dot{\theta}_c\right)^2 + \frac{1}{2}J_{c_y}\left(\dot{\psi}_c\right)^2 + \frac{1}{2}J_{c_z}\left(\dot{\phi}_c\right)^2 \\
& + \frac{3}{2}m_p[((r_c\cos(\phi_c) - r_c\dot{\phi}_c\sin(\phi_c))\dot{\phi}_c + (\dot{x}_p - c_1\omega_p\sin(\omega_p t)))^2 \\
& + ((r_c\sin(\phi_c) - r_c\dot{\phi}_c\cos(\phi_c))\dot{\phi}_c + \left(\dot{y}_p + c_1\omega_p\cos(\omega_p t)\right))^2] \\
& + \frac{3}{2}J_{pz}\left(\dot{\phi}_p\right)^2 \\
& + \frac{1}{2}m_s\left[\left(\dot{x}_s - d_1\omega_s\sin(\omega_s t)\right)^2 + \left(\dot{y}_s + d_1\omega_s\cos(\omega_s t)\right)^2\right] \\
& + \frac{1}{2}J_{s_x}\left(\dot{\theta}_s\right)^2 + \frac{1}{2}J_{s_y}\left(\dot{\psi}_s\right)^2 + \frac{1}{2}J_{s_z}\left(\dot{\phi}_s\right)^2 \\
& + \frac{1}{2}m_{g1}\left[\left(\dot{x}_{g1} - e_1\omega_{g1}\sin(\omega_{g1} t)\right)^2 + \left(\dot{y}_{g1} + e_1\omega_{g1}\cos(\omega_{g1} t)\right)^2\right] \\
& + \frac{1}{2}J_{g1_x}\left(\dot{\theta}_{g1}\right)^2 + \frac{1}{2}J_{g1_y}\left(\dot{\psi}_{g1}\right)^2 + \frac{1}{2}J_{g1_z}\left(\dot{\phi}_{g1}\right)^2 \\
& + \frac{1}{2}m_{g2}\left[\left(\dot{x}_{g2} - f_1\omega_{g2}\sin(\omega_{g2} t)\right)^2 + \left(\dot{y}_{g2} + f_1\omega_{g2}\cos(\omega_{g2} t)\right)^2\right] \\
& + \frac{1}{2}J_{g2_z}\left(\dot{\phi}_{g2}\right)^2 \\
& + \frac{1}{2}m_{g3}\left[\left(\dot{x}_{g3} - g_1\omega_{g3}\sin(\omega_{g3} t)\right)^2 + \left(\dot{y}_{g3} + g_1\omega_{g3}\cos(\omega_{g3} t)\right)^2\right] \\
& + \frac{1}{2}J_{g3_x}\left(\dot{\theta}_{g3}\right)^2 + \frac{1}{2}J_{g3_y}\left(\dot{\psi}_{g3}\right)^2 + \frac{1}{2}J_{g3_z}\left(\dot{\phi}_{g3}\right)^2 \\
& + \frac{1}{2}m_{GN}\left[\left(\dot{x}_{GN} - h_1\omega_{GN}\sin(\omega_{GN} t)\right)^2 + \left(\dot{y}_{GN} + h_1\omega_{GN}\cos(\omega_{GN} t)\right)^2\right]
\end{aligned}$$

$$+\frac{1}{2}J_{GN_x}\left(\dot{\theta}_{GN}\right)^2+\frac{1}{2}J_{GN_y}\left(\dot{\psi}_{GN}\right)^2+\frac{1}{2}J_{GN_z}\left(\dot{\phi}_{GN}\right)^2 \quad (19)$$

$$\begin{aligned}V=&\frac{1}{2}k_{LSS_x}\left(\delta\theta_{rc}\right)^2+\frac{1}{2}k_{LSS_y}\left(\delta\psi_{rc}\right)^2+\frac{1}{2}k_{LSS_z}\left(\delta\phi_{rc}\right)^2\\&+\frac{1}{2}k_{IS_x}\left(\delta\theta_{sg1}\right)^2+\frac{1}{2}k_{IS_y}\left(\delta\psi_{sg1}\right)^2+\frac{1}{2}k_{IS_z}\left(\delta\phi_{sg1}\right)^2\\&+\frac{1}{2}k_{HSS_x}\left(\delta\theta_{g3GN}\right)^2+\frac{1}{2}k_{HSS_y}\left(\delta\psi_{g3GN}\right)^2+\frac{1}{2}k_{HSS_z}\left(\delta\phi_{g3GN}\right)^2\\&+\frac{3}{2}k_{rp}\left(\delta_{rp_x}\right)^2+\frac{3}{2}k_{rp}\left(\delta_{rp_y}\right)^2+\frac{3}{2}k_{sp}\left(\delta_{sp_x}\right)^2+\frac{3}{2}k_{sp}\left(\delta_{sp_y}\right)^2\\&+\frac{1}{2}k_{g12}\left(\delta_{g12_x}\right)^2+\frac{1}{2}k_{g34}\left(\delta_{g34_x}\right)^2\\&+\frac{1}{2}k_{b1}\left(\delta x_{b1}\right)^2+\frac{1}{2}k_{b1}\left(\delta y_{b1}\right)^2+\frac{1}{2}k_{b2}\left(\delta x_{b2}\right)^2+\frac{1}{2}k_{b2}\left(\delta y_{b2}\right)^2\\&+\frac{3}{2}k_{b3}\left(\delta x_{b3}\right)^2+\frac{3}{2}k_{b3}\left(\delta y_{b3}\right)^2+\frac{1}{2}k_{b4}\left(\delta x_{b4}\right)^2+\frac{1}{2}k_{b4}\left(\delta y_{b4}\right)^2\\&+\frac{1}{2}k_{b5}\left(\delta x_{b5}\right)^2+\frac{1}{2}k_{b5}\left(\delta y_{b5}\right)^2+\frac{1}{2}k_{b6}\left(\delta x_{b6}\right)^2+\frac{1}{2}k_{b6}\left(\delta y_{b6}\right)^2\\&+\frac{1}{2}k_{b7}\left(\delta x_{b7}\right)^2+\frac{1}{2}k_{b7}\left(\delta y_{b7}\right)^2+\frac{1}{2}k_{b8}\left(\delta x_{b8}\right)^2+\frac{1}{2}k_{b8}\left(\delta y_{b8}\right)^2.\end{aligned} \quad (20)$$

Using these kinetic, potential energy terms, we derived Lagrange's equation and equation of motion. Eqs. (21)-(23) are the process of deriving equation of motion. Q vector is generalized forces including gravity and external force.

$$L=T-V \quad (21)$$

(T : Kinetic energy, V : Potential energy)

$$\frac{d}{dt}\left(\frac{\delta L}{\delta \dot{q}_j}\right)-\frac{\delta L}{\delta q_j}=Q_j \qquad j=1,2,3\ldots36 \quad (22)$$

where $(Q_j=Q_g(t)+Q_{ext}(t))$

$$[J]\ddot{\vec{\phi}}+[C]\dot{\vec{\phi}}+[K]\vec{\phi}=Q_j\,. \quad (23)$$

2.3 Simulation

Table 1 shows basic information about the drivetrain. Except bending stiffness of shaft, all properties are referred from Ref. [5]. About bending stiffness of shaft, we derived spring stiffness by the Timoshenko beam theory which assumes that the potential energy and spring potential energy have same magnitude [16]. Its derivation was explained in Eqs. (10) and (11).

About the environment, it was assumed that the aerodynamic torque is T_{aero} = 15000 N·m, and electromagnetic torque is -30 % of aerodynamic torque which corresponds 30 % wind turbine efficiency. The rotor was exited with the angular velocity of 6 rpm. About numerical method, the Newmark integration method was used [20, 21].

Table 1. Data for the drivetrain configuration presented in this work.

J_{rz} – inertia of the rotor (kg·m^2)	$4.18\cdot10^6$
J_{cz} – inertia of the carrier (kg·m^2)	57.72
J_{pz} – inertia of the planet (kg·m^2)	1.12
J_{sz} – inertia of the sun (kg·m^2)	0.86
J_{g1z} – inertia of the gear 1 (kg·m^2)	14.32
J_{g2z} – inertia of the gear 2 (kg·m^2)	1.62
J_{g3z} – inertia of the gear 3 (kg·m^2)	0.20
J_{GNz} – inertia of the generator (kg·m^2)	93.22
k_{LSSx} – bending stiffness about x-axis of the LSS (Nm/rad)	$1.34\cdot10^8$
k_{LSSy} – bending stiffness about y-axis of the LSS (Nm/rad)	$1.34\cdot10^8$
k_{LSSz} – torsional stiffness about z-axis of the LSS (Nm/rad)	$7.19\cdot10^7$
k_{ISx} – bending stiffness about x-axis stiffness of the IS (Nm/rad)	$2.48\cdot10^7$
k_{ISy} – bending stiffness about y-axis stiffness of the IS (Nm/rad)	$2.48\cdot10^7$
k_{ISz} – torsional stiffness about z-axis stiffness of the IS (Nm/rad)	$1.40\cdot10^7$
k_{HSSx} – bending stiffness about x-axis of the HSS (Nm/rad)	$2.83\cdot10^6$
k_{HSSy} – bending stiffness about y-axis of the HSS (Nm/rad)	$2.83\cdot10^6$
k_{HSSz} – torsional stiffness about z-axis of the HSS (Nm/rad)	$0.15\cdot10^7$
k_{rp}, k_{sp} – stiffness of the engaging tooth pairs in the low speed planetary gear stage (N/m)	$0.73\cdot10^8$
k_{g12} – stiffness of the engaging tooth pairs in the 1st high-speed parallel gear stage (N/m)	$2.02\cdot10^9$
k_{g34} – stiffness of the engaging tooth pairs in the 2nd high-speed parallel gear stage (N/m)	$0.11\cdot10^8$
r_c – radius of carrier (mm)	270
r_p – radius of planet (mm)	160
r_s – radius of sun (mm)	110
r_{g1} – radius of gear 1 (mm)	290
$r_{g2\text{-}1}$ – radius of gear 2_1 (mm)	95
$r_{g2\text{-}2}$ – radius of gear 2_2 (mm)	185
r_{g3} – radius of gear 3 (mm)	80
α – pressure angle (°)	20
Gear ratio	34.654

3. Results and discussion

3.1 Angular displacement comparison between torsional model and 3-dimensional model

The biggest difference between torsional and 3-dimensional model is that rotation and translation motion are coupled. In torsional model, we just thought about each rotation occurred by shaft stiffness and gear mesh which is related only rotation coordinates. However, rotation and translation are totally coupled by bearing, shaft in the 3-dimensional model.

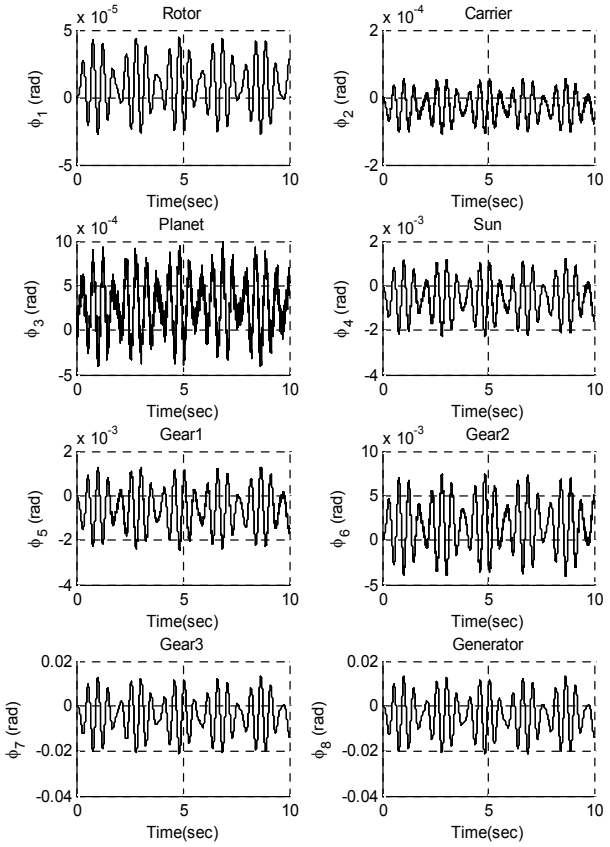

Fig. 3. Angular displacement difference between torsional model and 3D model.

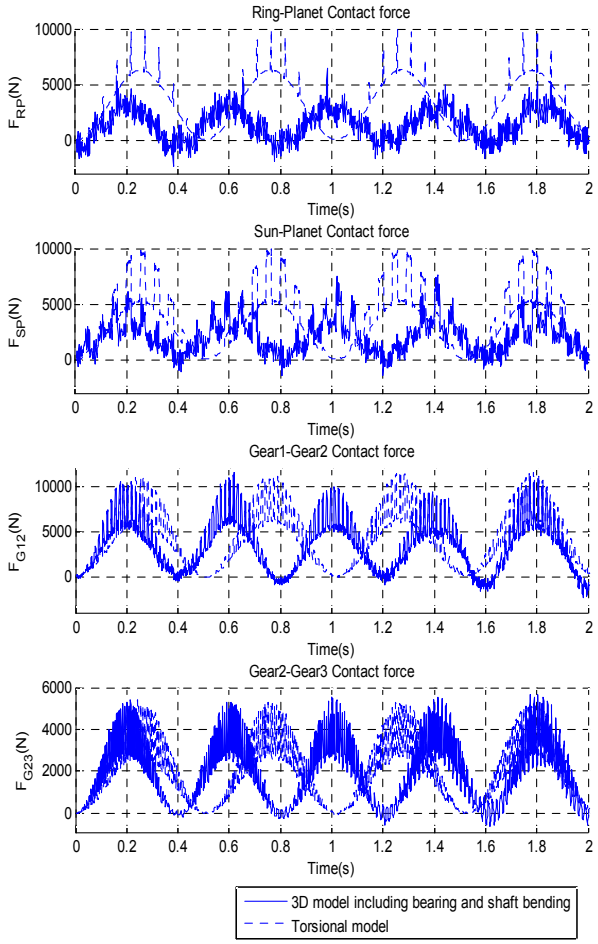

Fig. 4. Gear mesh contact force comparison between torsion model and 3D model.

These coordinates always affect each other. So we expected coupled vibrations which come from other component.

Through these facts, Fig. 3 shows the difference of rotational displacement about z-axis between the torsional model and the 3-dimensional model. Actually, if we see displacements closely, these are not curved line. It is always vibrating according reference line. In Fig. 3, there are periodic vibrations with their mean value close to zero. The magnitudes of vibration are getting larger through drivetrain because of gear ratio. Through this result, we estimated that vibrations of each component have similar shape and period. To see more detail, we expanded results into gear mesh.

3.2 Contact force comparison between torsional model and 3-dimensional model

Gear mesh is not only most important part in the mechanical system and but also one of risk part. If external force is bigger than acceptable force, gear teeth will be defected. In this chapter, we compared gear mesh contact force by same method. Fig. 4 represents gear mesh contact force plot in time domain.

In the 3D model, the contact force period is shorter than torsional model. This period means vibration about rotation direction. In other words, there are differences of angular velocity ratios between gears, because of shaft stiffness and gear mesh stiffness. This difference occurs that two points, which gear mesh takes place, will not meet and go away regularly. If two points meet regularly, the periodic vibration will not appear and has same shape of gear mesh stiffness as Fig. 1.

From these reasons, we got the regular contact force plots in the torsional model. Minimum value of contact force is 0. It perfectly shows that two points are not affected when two points sufficiently fall away. However, this phenomenon does not match in the 3D model. Because of coupled motion by bearing and shaft bend, the vibration is not regular and occasionally has minus value of contact force. In theoretically, the contact force has constant direction, and two points meet and go away in gear relation. However, the existence of bearing and shaft bending causes disturbance which makes additional relation between gear teeth, when the gear tooth sufficiently fall away. This is the cause of minus contact force values.

Before simulation, we expected that there is more vibration between gear 1 and gear 2, because it has the biggest gear mesh stiffness and gear radius ratio written in Table 2. However, irregular vibrations took place frequently in the planetary gear stage compared to parallel gear stages.

Through this fact, we concluded that planetary gear takes more influences of shaft bending. In the drivetrain, Sun gear

Table 2. Gear radius ratios and average of gear mesh stiffness.

	Planet-sun	Gear1-gear2	Gear2-gear3
Radius ratio	1.4545	3.0526	2.3125
Average of gear mesh stiffness	$0.73 \cdot 10^8$ N/m	$2.02 \cdot 10^9$ N/m	$0.11 \cdot 10^8$ N/m

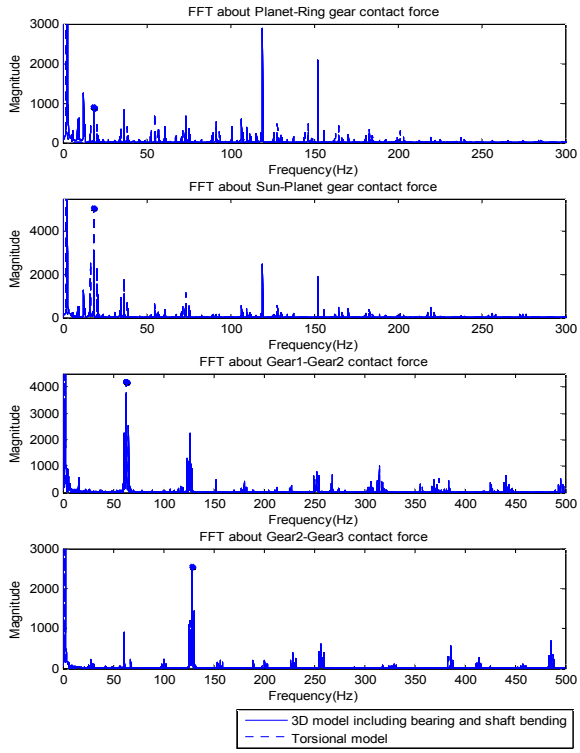

Fig. 5. Fourier transform of gear mesh contact force.

and planet gears are connected by low speed shaft and Intermediate shaft. Also the number of planet gear is 3, although parallel gear has two gears. This geometric fact represents that planetary gear stage has more risk and coincides with gear mesh contact force results.

In Fig. 5, we transformed gear mesh contact force into frequency domain. Gear mesh frequencies and harmonic terms can be founded and checked as dot in plot. 18.31 Hz in planetary gear stages, 63.12 Hz in the gear 1-gear 2 and 128.6 Hz in the gear 2-gear 3 are dominant and each harmonic terms multiply 2,3,4…,n are represented. These values are same to angular velocities which were defined in Eqs. (1)-(3). The basic frequencies of 2.5 Hz for 3D model and 2.0 Hz for torsional model can be found from Fig. 5. These frequencies are related to the periodic gear mesh stiffness of the planetary gear system. The difference between 3D model and torsional model may be caused by the gear backlash due to the bending of the shaft.

The reason that gear 2- gear 3 has higher gear mesh frequency is high angular velocity compared others. Although gear contact of ring-planet and planet-sun have different stiff-

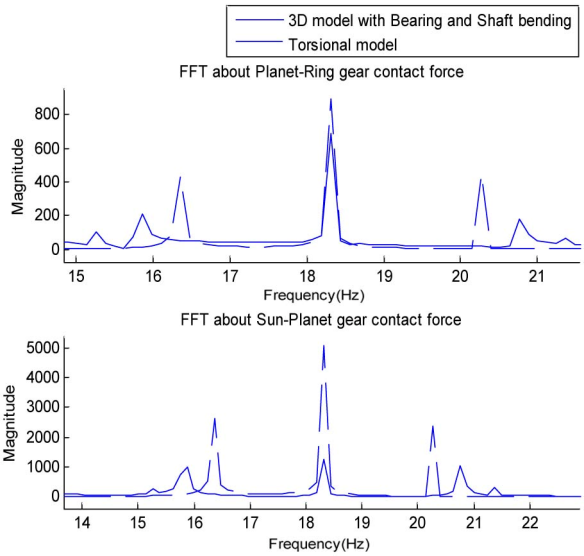

Fig. 6. Comparison of gear mesh frequency and sideband frequencies.

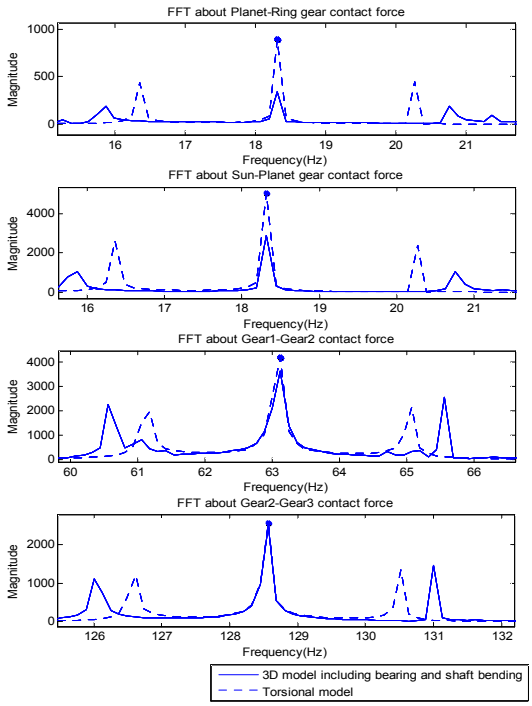

Fig. 7. Comparison of sideband frequencies.

ness model, these show same gear mesh frequencies.

In the 3D model, there are irregular peaks. This is another evidence of coupled motion. Through this fact, it is necessary to consider shaft flexibility. However, coupled relative motion can create additional vibration peak, but main characteristic of system doesn't change. Fig. 6 shows gear mesh frequency and side band peak closely. As you can see, the location of gear mesh frequency is same and sidebands are changed. More clearly, sidebands distance is longer than torsional model. In

other words, the system has faster and longer rotating frequency signals compared to torsional model.

Through this fact, we can expect that if there is shaft bending effect or eccentricity problem, the gear mesh contact period will be short and irregular small vibration will appear.

To verify this fact, we compared our model to the Ref. [22]. In the reference, there are additional sideband peaks around gear mesh frequency in gear eccentricity, backlash, and bearing problems. And the magnitudes of couples of side peak are different.

Fig. 7 shows the planetary gear stage's sideband frequencies around gear mesh frequency. As you can see, we found same patterns of additional sideband peaks around gear mesh frequency as explained in reference. And the magnitudes of sidebands also are different. From these results, we can conclude shaft bending causes improper backlash and eccentricity problems.

4. Conclusions

A 3-dimensional mathematical model of drivetrain including shaft bending effect was proposed. Especially, it suggested bending deflection of shaft, eccentricity compared previous researches. Using this mathematical model, we simulated according assumptions and environments. Finally, we showed dynamics responses, compared to torsional model, reference model, explained effect of shaft bending, and concluded its physical meaning and phenomenon.

By addition of degree of freedom about bending axis, the gear mesh contact force was affected. As a result, irregular vibration take place and gear teeth always take loads even though two gear tooth fall away. If shaft is bended in manufacturing, it will produce abnormal loads. Especially, planetary gear stages are more sensitive compared parallel gear stages because of geometry.

Planetary gear stage is composed of planet, sun, ring gears. In case by case, its number of gears and rotation angle can be defined by users. Planet gears can take lots of loads from input torque. It transfers torque to sun gear. The number of planet gear determines capacity of planetary gear stage. A lot of planet gears can divide high load. As a result, planetary gear stage's capacity is higher. Vice versa, if there is un-parallel problem such as shaft bending, eccentricity, its effect will be higher. As referred in this work, in the drive train system, low speed shaft and intermediate shaft should be checked regularly. Also, eccentricity and products line misalignment problem should be considered.

Although there are a lot of vibrations in gear mesh contact force, the location of gear mesh frequencies are not changed. In other words, external or relative component's disturbances just affect sidebands location and magnitude. However general gear mesh contact force has same shape and trend. Therefore, using this mathematical model, we need to research how it will affect gear tooth in elastic and plastic deformation aspect.

Acknowledgments

The authors would like to gratefully acknowledge financial support from the National Science Foundation of China (Grant No. 51709039, 51379032, 51761135011, 51490672 and 51679036) and Royal Academy of Engineering under the UK-China Industry Academia Partnership Program (Grant No.UK-CIAPP\73). This work is also partially supported by Innovation Fund for Young Scholars from State Key Laboratory of Coastal and Offshore Engineering, Dalian University of Technology (LY17B3).

Nomenclature

$a1, b1, c1, d1, e1, f1, g1$: Radius of unbalanced mass
g : Gravity acceleration
T : Kinetic energy
V : Potential energy
L : Lagrange equation
N : Gear ratio
C_{rp}, C_{rs} : Gear contact ratio
γ_{rp} : Planet Gear's gear mesh angle
q : Generalized coordinate
$[J]$: Mass matrix
$[K]$: Stiffness matrix
$[C]$: Damping matrix
$[Q]$: Generalized force
$[Q_g]$: Gravity
$[Q_a]$: External force
Φ : Degree of freedom

References

[1] Y. J. Park, J. G. Kim, G. H. Lee and S. B. Shim, Load sharing and distributed on the gear flank of wind turbine planetary gearbox, *Journal of Mechanical Science and Technology*, 29 (1) (2015) 309-316.

[2] C. C. Zhu, S. Chen, C. S. Song, H. J. Liu, H. Y. Bai and F. Ma, Dynamic analysis of a megawatt wind turbine drive train, *Journal of Mechanical Science and Technology*, 29 (5) (2015) 1913-1919.

[3] J. S. Nam, Y. J. Park and H. S. Chang, Dynamic life prediction of pitch and yaw bearings for wind turbine, *Journal of Mechanical Science and Technology*, 30 (1) (2016) 249-256.

[4] W. Shi, C. W. Kim, C. W. Chung and H. C. Park, Dynamic modeling and analysis of a wind turbine drivetrain using the torsional dynamic model, *International Journal of Precision Engineering and Manufacturing*, 14 (1) (2013) 153-159.

[5] M. Todorov and G. Vukov, Parametric torsional vibrations of a drive train in horizontal axis wind turbine, *1st Conference Franco-Syrian about Renewable Energy*, Damas, Syrie, Oct. 24-28 (2010).

[6] Y. Guo, J. Keller and W. LaCava, Combined effects of gravity, bending moment, bearing clearance, and input torque on wind turbine planetary gear load sharing, *American Gear*

Manufacturers Association Technical Paper, 12FTM05 (2012).
[7] Q. Zhang, J. H. Kang, W. Dong and S. K. Lyu, A study on tooth modification and radiation noise of manual transaxle, *International Journal of Precision Engineering and Manufacturing*, 13 (6) (2012) 1013-1020.
[8] B. Shlecht, T. Shulze and T. Rosenlocher, Simulation of heavy drive trains with multimegawatt transmission power in SimPACK, *SIMPACK Users Meeting* (2006).
[9] M. Todorov and G. Vukov, Modal properties of drive train in horizontal-axis wind turbine, *Proc. of International Conference on Innovations, Recent Trends And Challenges In Mechastonics, Mechanical Engineering And New High-Tech Products Development- MECAHITECH'11*, Bucharest, Romania, 22-23 September (2011).
[10] D. H. Lee, D. H. Hodges and M. J. Patil, Multi-flexible-body dynamic analysis of horizontal axis wind turbines, *Wind Energy*, 5 (2002) 281-300.
[11] R. C. Juvinall and K. M. Marshek, *Fundamentals of machine component design*, Fifth Ed., John Wiley & Sons, New York, USA (2011).
[12] F. L. J. vander Linden and P. H. V. de Souza Silva, Modelling and simulating the efficiency and elasticity of gearboxes, *Proc. of 7th Modelica Conference*, Como, Italy (2009) 270-277.
[13] J. H. Wang, D. T. Qin and Y. Ding, Dynamic behavior of wind turbine by a mixed flexible-rigid multi-body model, *Journal of System Design and Dynamics*, 3 (3) (2009) 403-419.
[14] A. Shabana, *Computational dynamics*, John Wiley & Sons, New York, USA (2010).
[15] A. K. Chopra, *Dynamics of structures: Theory and applications to earthquake engineering*, Prentice Hall, New Jersey, USA (2001).
[16] S. Y. Jiang and S. Z. Duan, A four-rigid-body element model and computer simulation for flexible components of wind turbines, *Proc. of the ASME 2011 International Mechanical Engineering Congress & Exposition*, Denver, USA (2011) 935-942.
[17] H. W. Kim and W. S. Yoo, Selection of damping model in vibration of flexible beams, *Proc. of KSME Fall Conference*, Jeju, Korea (2007) 3538-3543.
[18] S. S. Rao, *Mechanical vibrations*, 4th Ed., Prentice Hall, New Jersey, USA (2004).
[19] R. R. Craig Jr. and A. J. Kurdila, *Fundamentals of structural dynamics*, John Wiley & Sons, New York, USA (2006).
[20] K. J. Bathe, *Finite element procedures*, Prentice Hall, New Jersey, USA (1996).
[21] Y. D. Kim, C. W. Kim, S. J. Lee and H. C. Park, Dynamic modeling and numerical analysis of a cold rolling mill, *International Journal of Precision Engineering and Manufacturing*, 14 (3) (2013) 407-413.
[22] R. K. Mobley, *An introduction to predictive maintenance*, Second Ed., Butterworth Heinmann, USA (2002).

Wei Shi received his B.S. degree from Yanbain University, China, in 2006, and Ph.D. degree from Pohang University of Science & Technology, Korea, in 2013. He is currently an Associate Professor at Dalian University of Technology in China. His research interests include drivetrain dynamics, offshore wind turbine dynamics.

Yonghui Park got Ph.D. degree from Pohang University of Science & Technology, South Korea in 2014. Currently he is a Researcher at the Pohang Institute of Metal Industry Advancement. His current research interests are analysis of mechanical system using the multi-body dynamics, and new design solution by reliability based design optimization.

Hyunchul Park received his B.S. degree from Seoul National University, South Korea in 1974, and M.S., Ph.D. degrees from University of IOWA, USA, in 1981 and 1985. He is currently a Professor at the Graduate School of Engineering mastership at Pohang University of Science & Technology.

Dezhi Ning received his Ph.D. degrees from Dalian University of Technology, China, in 2005. He is currently a Professor at the State Key Laboratory of Coastal and Offshore Engineering, Dalian University of Technology.